Berry curvature force and Lorentz force comparison in the magnetotransport of Weyl semimetals

Muhammad Imran and Selman Hershfield
Department of Physics, University of Florida, Gainesville, Florida 32611, USA

(Received 4 April 2018; revised manuscript received 3 August 2018; published 19 November 2018)

Three-dimensional Weyl semimetals have been observed to have negative magnetoresistance (MR) with the magnetic field parallel to the electric field and positive MR with the magnetic field perpendicular to the electric field. It is understood that the negative MR is due to a Berry phase that causes the chiral anomaly, while the positive MR can be understood from a semiclassical transport theory. We solve a semiclassical Boltzmann equation with both the Berry phase and Lorentz force terms present for an arbitrary angle of the applied magnetic field relative to the electric field within the relaxation-time approximation. The plots of the magnetoconductivity show both the Berry phase and Lorentz force effects. For some angles between the electric and magnetic fields, the conductivity has a minimum, where the forces balance each other. The standard semiclassical theory does not show the linear increase in the transverse MR with the magnetic field seen experimentally. By assuming a magnetic-field-dependent transport time, we find the transverse MR increases linearly with the magnetic field. The low-field MR does change from negative to positive as one rotates the magnetic field away from the direction of the electric field. As the magnetic field is increased, we find in some cases the MR starts out negative and then becomes positive. This is consistent with recent experimental data in Cd_3As_2.

DOI: 10.1103/PhysRevB.98.205139

I. INTRODUCTION

Weyl fermions (WFs) are the zero-mass solution of the Dirac equation. They have been well studied theoretically in high-energy physics, but it has remained experimentally a challenge to find a Weyl fermion fundamental particle [1–3]. The experimental discovery of graphene with a gapless energy spectrum was a milestone towards realizing Weyl fermions [4]; however, the pseudospin and momentum coupling in graphene is incomplete, and graphene states are fragile to perturbations. The search for topologically protected gapless Weyl fermions, even in condensed-matter physics, has had many ups and downs. By using *ab initio* calculations many materials were predicted to host these topological states [5–8].

At this point there is strong experimental evidence for Weyl fermions in a number of materials. Angle-resolved photoemission spectroscopy (ARPES), soft x rays, scanning tunneling microscopy, and magnetotransport measurements have become the test beds to detect the elusive WF states [9–11]. Most of these experimental results are also verified by the *ab initio* calculations and minimal Hamiltonian models [12,13]. The massless WFs travel with Fermi velocity $v_F \sim 10^8$ cm/s, which is much smaller than the speed of the light. In fact, the Lorentz symmetry in condensed matter is an artifact of making the band structure linear near the Dirac points. Thus, the Lorentz symmetry is allowed to be violated, unlike the Lorentz symmetry in special relativity. The Weyl semimetals are categorized as type-I and type-II materials, depending upon their Fermi surface at the band touching point. The type-I Weyl semimetals have one point where conduction and valance bands meet, whereas in type-II Weyl semimetals electrons and holes pockets meet, and they form an open Fermi surface [14]. For a discussion on type-I and type-II Weyl fermions, see Refs. [15–17].

Weyl semimetals are different from topological insulators, which emerge due to the strong spin-orbit interaction [18]. Three-dimensional topological insulators are novel states of matter with insulating bulk and topologically protected surface states. In contrast, the bulk and surface states of the Weyl semimetals are both topologically protected [9]. The unique surface states of the Weyl semimetals make nonclosed Fermi arcs that terminate in the bulk. The nontrivial topology of the band structure of WFs gives rise to the nontrivial Berry curvature physics of the WF [19]. The Weyl nodes are the source and sink of Berry magnetic field in momentum space. In the crystal lattice structures the WFs could emerge in the absence of time-reversal or inversion symmetry [20,21]. By breaking the time-reversal symmetry [10] or the spatial-inversion symmetry [11] the WF pairs are detected in ARPES experiments [9].

The magnetotransport properties of Weyl fermions include the chiral magnetic effect [22–25], the anomalous Hall effect [26], and negative magnetoresistance [27]. The negative magnetoresistance is related to the chiral anomaly, which is one of the signatures of a Weyl semimetal. The chiral anomaly is the violation of the conservation law of the chiral current [10,28]. In a weak magnetic field and in the high-temperature limit, the longitudinal resistivity in the direction of magnetic field is shown to decrease quadratically with the magnetic field [27]. This phenomenon is observed for samples with low density to keep the Fermi level close to WF points.

In this study we compare the relative effects of the Lorentz force and the force due to Berry curvature in magnetotransport derived from the Boltzmann equation. This is achieved by changing the relative angle between the electric field and the magnetic field. The diagonal elements of the transverse magnetoconductivity tensor decrease quadratically with the

magnetic field due to the Lorentz force effect. However, the longitudinal magnetoconductivity (MC) increases with the magnetic field due to the Berry curvature force effect. Here transverse and longitudinal are used as a reference to the direction of magnetic field. Therefore, by rotating the electric field away from the magnetic field axis, the diagonal elements of the magnetoconductivity tensor plot pass through a minimum point. At this minimum point the Lorentz force and the force of the Berry curvature effectively cancel each other. The situation is different for the magnetoresistance. The effect of the Lorentz force is absent in the diagonal elements of the transverse magnetoresistance (TMR) tensor, and therefore, a comparison between these forces is not possible.

Interestingly, the TMR data from Weyl semimetals do not stay constant with the magnetic field [29]. The TMR is shown to increase linearly with increasing magnetic field [30], in contrast to a formal theory of the Boltzmann equation in the relaxation-time approximation. In this paper we phenomenologically include the magnetic field dependence in the relaxation process of the distribution function in order to obtain a TMR which increases linearly with magnetic field. The magnetic field dependence of the TMR has been an active area of research in Dirac and Weyl semimetals in both the ultraquantum and semiclassical limits of studies [31,32]. In this study we are assuming the magnetic-field-dependent transport time within a semiclassical region.

In Sec. II of this paper we present the theoretical formulation of magnetotransport through Weyl semimetals; Sec. III is reserved for numerical results of our model, and we give our conclusions in Sec. IV.

II. THEORETICAL FORMULATION

This study focuses on the case when both the Lorentz force and Berry curvature force are important in the magnetotransport in Weyl fermions. The inclusion of Berry curvature in a semiclassical study modifies its equations of motion by introducing the change in phase space, adding an anomalous velocity and a force that is directly proportional to the Berry curvature (we shall use the term Berry force for this force) [30,33–35]. Research has already been carried out on the magnetotransport in Weyl fermions [27,36–40]. From this work we know that the negative magnetoresistance in Weyl fermions can be explained by Berry curvature. Along with this, the conductivity should show a comparison between the Lorentz and Berry curvature forces within the plane of applied fields. Berry curvature is a physical quantity of the Bloch wave function defined for a crystal lattice structure that lacks either the inversion symmetry [10] or the time-reversal symmetry [11]. The semiclassical equations of motion in the presence of the Berry curvature are a well-studied problem [30,41,42]. We are interested in the magnetotransport of a semiclassical WF gas described by the linearized energy spectrum of an energy band structure near the Dirac points. The Dirac points are degenerate due to Kramer's rule. By applying an external magnetic field, the Landau levels are formed, and Kramer's degeneracy is lifted.

A. The semiclassical theory of magnetotransport in the Weyl semimetals

The well-studied Hamiltonian of the Weyl fermions is [43–45]

$$H_k = \chi v_F \hbar[(\vec{k} - \chi \vec{Q}) \cdot \vec{\sigma} + \sigma_0 Q_0]. \tag{1}$$

Here σ are Pauli spinors and denote real spins, and $\chi = \pm$ is used to include chirality. The parameter $\vec{Q}$ (Q_0) breaks time-reversal symmetry (inversion symmetry) and splits degenerate Dirac cones in momentum (energy) space [43]. We consider $Q_0 = 0$, and $\vec{Q} = Q_z\hat{z}$. In a semiclassical theory the magnetic field enters from the Boltzmann equation since the Landau levels are not resolved. The eigenvalues of this Hamiltonian are

$$E_k(\pm, \chi) = \pm \hbar k(\chi) v_F, \quad k(\chi) = \sqrt{k_\perp^2 + (Q_z + \chi k_z)^2}, \tag{2}$$

where $\chi = \pm 1$ and $k_\perp = \sqrt{k_x^2 + k_y^2}$. The semiclassical dynamics of a Bloch wave packet in the presence of electric and magnetic fields is derived in the Appendix (see also Refs. [29,33,34] for the derivation and application of these equations):

$$\dot{\vec{x}} = A\left[\vec{v} - \frac{e}{\hbar}\vec{E} \wedge \vec{\Omega} + \frac{e}{\hbar}(\vec{\Omega} \cdot \vec{v})\vec{B}\right], \tag{3}$$

$$\hbar\dot{\vec{k}} = A\left[e\vec{E} + e\vec{v} \wedge \vec{B} + \frac{e^2}{\hbar}(\vec{E} \cdot \vec{B})\vec{\Omega}\right], \tag{4}$$

where $\dot{x}$, $\hbar\dot{k}$, and $A = (1 + \frac{e}{\hbar}\vec{B} \cdot \vec{\Omega})^{-1}$ are the mean velocity, forces, and change in phase space for Berry curvature, respectively.

To make a comparative analysis of the Berry curvature force and the Lorentz force, we write the semiclassical Boltzmann equation with uniform-in-space and time-independent electric and magnetic fields perturbing a system of Weyl particles, which includes both electrons and holes:

$$\vec{F} \cdot \frac{1}{\hbar}\vec{\nabla}_k f_\chi = I[\text{coll}],$$
$$\vec{F} = -eA\left[\vec{E} + \frac{e}{\hbar}(\vec{E} \cdot \vec{B})\vec{\Omega} + \vec{v} \times \vec{B}\right]. \tag{5}$$

Here f_χ is the distribution function, $I[\text{coll}]$ is the collision integral of a Boltzmann equation, $\vec{E}$ and $\vec{B}$ are the electric and magnetic fields, and $\vec{v} = \pm v_F\hat{k}$ is the group velocity of the Dirac spectrum. The force term has the usual electric and magnetic forces as well as a force arising due to Berry curvature ($\vec{\Omega} = \chi\frac{\vec{k}}{2k^3}$). This force also displaces the sphere of the Weyl gas out of equilibrium, and therefore, charge transport parameters such as the thermal and electrical conductivities depend on this force. We assume a linear response in the electric field for the nonequilibrium distribution function and use the relaxation-time approximation for the Weyl particle gas sphere to fall back into equilibrium: $I[\text{coll}] = -\frac{\delta f_\chi}{\tau_{tr}}$,

$$-e\vec{E} \cdot \vec{v}\frac{\partial f_{eq}}{\partial E_k} - \frac{e^2}{\hbar}(\vec{E} \cdot \vec{B})(\vec{\Omega} \cdot \vec{v})\frac{\partial f_{eq}}{\partial E_k},$$
$$-e\vec{v} \times \vec{B} \cdot \frac{1}{\hbar}\vec{\nabla}_k \delta f_\chi = -\frac{\delta f_\chi}{A\tau_{tr}}. \tag{6}$$

Here $f_{eq} = \{1 + \exp[\beta(E_k - \mu)]\}^{-1}$ is the Fermi Dirac distribution function, $\beta^{-1} = k_B T$ denotes the thermal energy of the Weyl fermions, and the symbol μ is used for the chemical potential. In the above equation we have used the vector identity $\vec{v} \times \vec{B} \cdot \vec{v} \frac{\partial f_{eq}}{\partial E_k} = 0$ in the last term on the left-hand side of the Boltzmann equation.

As we are dealing with fermions, we make an ansatz in which the deviation of the equilibrium distribution function from equilibrium is projected close to the Fermi energy, $\delta f_\chi = g_\chi(-\partial f_{eq}/\partial E_k)$. The equation for g_χ is

$$e\vec{E} \cdot v_F \frac{\vec{k}}{|k|} + \chi \frac{e^2 v_F E_z B_z}{2\hbar|k|^2} = e v_F \frac{\vec{k}}{|k|} \times \vec{B} \cdot \frac{1}{\hbar} \vec{\nabla}_k g_\chi - \frac{g_\chi}{A\tau_{tr}}. \tag{7}$$

Here the wave vector in spherical coordinates is $\hat{k} = \vec{k}/|k| = \cos\theta \hat{z} + \sin\theta(\sin\phi \hat{y} + \cos\phi \hat{x})$. Expanding g_χ in Fourier harmonics,

$$g_\chi = \sum_n \left[\alpha_n^\chi \cos(n\phi) + \beta_n^\chi \sin(n\phi)\right]. \tag{8}$$

To find the coefficients α_n^χ and β_n^χ we use the orthonormality of Fourier components. All coefficients with $n > 1$ are zero. Our final result for g_χ is

$$\begin{aligned} g_\chi = & -e v_F \tau_{tr} E_z \frac{2E_k^2 \cos\theta + \chi e B_z \hbar v_F^2}{2E_k^2 + \chi e B_z \hbar v_F^2 \cos\theta} \\ & - \frac{2e v_F \tau_{tr} E_k \sin\theta}{\left(2eE_k B_z \tau_{tr} v_F^2\right)^2 + \left(2E_k^2 + \chi e B_z \hbar v_F^2 \cos\theta\right)^2} \\ & \times \Big(E_x \Big\{ \cos\phi \Big[E_k \left(2E_k^2 + \chi e B_z \hbar v_F^2 \cos\theta\right)\Big] \\ & + \sin\phi \left(2E_k^2 e B_z \tau_{tr} v_F^2\right)\Big\} + E_y \Big\{ \sin\phi \Big[E_k \left(2E_k^2 \right. \\ & \left. + \chi e B_z \hbar v_F^2 \cos\theta\right)\Big] - \cos\phi \left(2E_k^2 e B_z \tau_{tr} v_F^2\right)\Big\}\Big). \end{aligned} \tag{9}$$

Using this distribution function, one can evaluate the density, currents, and conductivities. It should be noted that the particle number is conserved:

$$\sum_{\chi=\pm} \int \frac{d^3k}{(2\pi)^3} A^{-1} \frac{\delta f_\chi}{\tau_{tr}} = \left(\frac{e}{h}\right)^2 \vec{E} \cdot \vec{B} \sum_{\chi=\pm} \chi = 0, \tag{10}$$

$$\frac{\partial}{\partial t}(N_+ + N_-) + \vec{\nabla} \cdot (\vec{J}_+ + \vec{J}_-) = 0. \tag{11}$$

The Berry curvature force induces an imbalance between the number density of the different chirality particles populations:

$$|\delta F| = \int \frac{d^3k}{(2\pi)^3} (\delta f_+ - \delta f_-), \tag{12}$$

where δF is the average difference in the deviation of the distribution function due to the chirality. With the distribution function in Eq. (9) this chirality imbalance is

$$\begin{aligned} |\delta F| = & \frac{e v_F \tau_{tr} E_z \beta}{2\pi^2 \hbar^3 v_F^3} \int_{-\infty}^{\infty} dE_k \left(\frac{4E_k^4}{e B_z \hbar v_F^2} + E_k^2 \frac{\left(e B_z \hbar v_F^2\right)^2 - 4E_k^4}{\left(e B_z \hbar v_F^2\right)^2} \right. \\ & \left. \times \ln \left| \frac{2E_k^2 + e B_z \hbar v_F^2}{2E_k^2 - e B_z \hbar v_F^2} \right| \right) \frac{1}{\cosh^2\left(\beta \frac{E_k - \mu}{2}\right)}. \end{aligned} \tag{13}$$

This average difference in the distribution function vanishes: $\delta F \to 0$ for $B \to 0$.

The current flowing through this system is

$$\vec{j} = -e \sum_\chi \int \frac{d^3k}{(2\pi)^3} A^{-1} \vec{\dot{x}} \delta f_\chi. \tag{14}$$

Note that in the above formula for the current, we have included the change in phase space factor due to the Berry curvature: $A = 2E_k^2/(2E_k^2 + \chi e B \hbar v_F^2 \cos\theta)$ [35]. The zz component of the conductivity is

$$\begin{aligned} \sigma_{zz} = & \frac{e^2 \tau_{tr} \beta}{32\pi^2 \hbar^3 v_F} \sum_\chi \int_{-\infty}^{\infty} dE_k \\ & \times \int_{-1}^{1} dy \frac{\left(2E_k^2 y + \chi e B \hbar v_F^2\right)^2}{2E_k^2 + \chi e B \hbar v_F^2 y} \frac{1}{\cosh^2\left(\beta \frac{E_k - \mu}{2}\right)}. \end{aligned} \tag{15}$$

Holes are included in the conductivity formula from the Weyl particle gas spectrum by changing $-e$ to e and E_k to $-E_k$. In a similar manner the other components of the conductivity tensor are found to be

$$\begin{aligned} \sigma_{xx} = & \frac{e^2 \tau_{tr} \beta}{16\pi^2 \hbar^3 v_F} \sum_\chi \int_{-\infty}^{\infty} dE_k \int_{-1}^{1} dy (1 - y^2) \\ & \times \frac{E_k^4 \left(2E_k^2 + \chi e B \hbar v_F^2 y\right)}{\left(2E_k^2 + \chi e B \hbar v_F^2 y\right)^2 + \left(2E_k e B \tau_{tr} v_F^2\right)^2} \\ & \times \frac{1}{\cosh^2\left(\beta \frac{E_k - \mu}{2}\right)}, \end{aligned} \tag{16}$$

$$\begin{aligned} \sigma_{xy} = & -\frac{e^2 \tau_{tr} \beta}{16\pi^2 \hbar^3 v_F} \sum_\chi \int_{-\infty}^{\infty} dE_k \int_{-1}^{1} dy (1 - y^2) \\ & \times \frac{2E_k^5 \left(e B \tau_{tr} v_F^2\right)}{\left(2E_k^2 + \chi e B \hbar v_F^2 y\right)^2 + \left(2E_k e B \tau_{tr} v_F^2\right)^2} \\ & \times \frac{1}{\cosh^2\left(\beta \frac{E_k - \mu}{2}\right)}. \end{aligned} \tag{17}$$

From σ_{zz}, σ_{xx}, and σ_{xy} one can obtain all the elements of the conductivity matrix using $\sigma_{yy} = \sigma_{xx}$ and $\sigma_{yx} = -\sigma_{xy}$.

In the limit of zero temperature, we give here the explicit formula for the conductivities and compare them with previous published work [33,46,47]:

$$\begin{aligned} \sigma_{zz} &= \frac{e^2 \mu^2}{3\pi\hbar^3 v_F} \frac{\tau_{tr}}{\pi} \left[1 + \frac{2}{5} \frac{1}{(l_B k_F)^4}\right], \\ \sigma_{xx} &= \frac{e^2 \mu^2}{3\pi\hbar^3 v_F} \frac{\tau_{tr}}{\pi} \left[1 - (\omega_c \tau_{tr})^2 + \frac{1}{20} \frac{1}{(l_B k_F)^4}\right], \\ \sigma_{xy} &= -\frac{e^2 \mu^2}{3\pi\hbar^3 v_F} \frac{\tau_{tr}}{\pi} (\omega_c \tau_{tr}) \left[1 - (\omega_c \tau_{tr})^2 + \frac{3}{20} \frac{1}{(l_B k_F)^4}\right]. \end{aligned} \tag{18}$$

Here $l_B^2 = \frac{\hbar}{e B_z}$ denotes the magnetic length. For our perturbation theory to be applied here, we consider $\omega_c \tau_{tr} < 1$ and $l_B k_F > 1$, $\mu = 10^2$ meV [47].

For zero magnetic field our results exactly match those in Refs. [48,49]. For a single Dirac cone we set $\sum_\chi = \frac{1}{2}$ and $\frac{\tau_{tr}}{\pi} = \delta(\Omega)$, and the conductivity $\sigma_{xx} = \sigma_{yy} = \sigma_{zz} = \frac{e^2 \mu^2}{6\pi\hbar^3 v_F} \delta(\Omega)$. For finite magnetic field, our result for conductivity $\delta\sigma_{zz} \sim B_z^2$ qualitatively agrees with Refs. [33,46], namely,

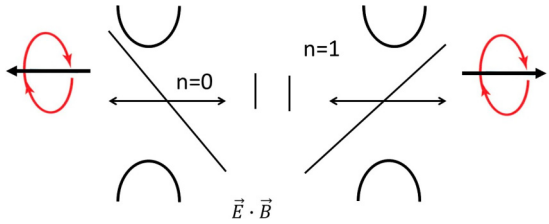

FIG. 1. The left- and right-handed chiral states of the $n = 0$ Landau level.

a quadratic increase in the conductivity with magnetic field due to the chiral anomaly.

The different elements of the resistivity matrix are found by taking the inverse of the conductivity matrix: $\rho_{zz} = 1/\sigma_{zz}$, $\rho_{xx} = \sigma_{yy}/(\sigma_{xx}^2 + \sigma_{xy}^2)$, $\rho_{yy} = \rho_{xx}$, $\rho_{xy} = \sigma_{xy}/(\sigma_{xx}^2 + \sigma_{xy}^2)$, and $\rho_{xy} = -\rho_{yx}$.

To do a comparative analysis of the force entering in a Boltzmann equation due to the Berry curvature and the Lorentz force, we use a rotation matrix to rotate the electric field [23,50]. These forces have counter effects in magnetoconductivity. The electric field is rotated from a plane perpendicular to the magnetic field to parallel to the magnetic field. For some angles the MC will change slope with magnetic field. For this particular value of the magnetic field, the Berry curvature and the Lorentz forces are balanced. The conductivity matrix from the above equations is

$$\begin{bmatrix} j_x \\ j_y \\ j_z \end{bmatrix} = \begin{bmatrix} \sigma_{xx} & \sigma_{xy} & 0 \\ \sigma_{yx} & \sigma_{yy} & 0 \\ 0 & 0 & \sigma_{zz} \end{bmatrix} \begin{bmatrix} E_x \\ E_y \\ E_z \end{bmatrix}. \tag{19}$$

When rotating about the y axis, the current, conductivity tensor, and electric field are transformed:

$$\vec{j}' = \hat{\sigma}'\vec{E}', \tag{20}$$

where $\vec{j}' = \hat{M}\vec{j}$, $\hat{\sigma}' = \hat{M}\hat{\sigma}\hat{M}^\dagger$, and $\vec{E}' = \hat{M}\vec{E}$. The rotation matrix is

$$\hat{M} = \begin{bmatrix} \cos\theta & 0 & -\sin\theta \\ 0 & 1 & 0 \\ \sin\theta & 0 & \cos\theta \end{bmatrix}. \tag{21}$$

The comparison between these forces is discussed in Sec. III.

B. The quantum theory of magnetotransport in Weyl semimetals

In the ultraquantum limit only the ground state of the $n = 0$ Landau level is populated (see Fig. 1). The Weyl fermion motion is frozen in the plane perpendicular to the magnetic field since $\frac{v_F\tau}{l_B} \gg 1$, $\frac{\hbar v_F}{l_B} > \mu, k_BT$. However, the fermions are free to move along the direction of the magnetic field. In an ideal case of only left- (chirality $\chi = -1$) or right- (chirality $\chi = +1$) handed Weyl fermions the presence of impurity would make conductivity zero in the direction of the magnetic field. However, the Weyl fermions have both left- and right-handed particles. These Weyl fermions scatter from the impurities and exchange their chirality state. This makes the conductivity finite. For instance, the left-handed Weyl fermions scatter from impurities and enter into a right-handed Weyl fermion state. The Weyl fermions scatter with impurities and relax their momentum by exchanging their chirality states with each other.

Here we use Kubo's formula to derive the conductivity in the ultraquantum limit of large magnetic field for Weyl fermions. The conductivity increases linearly with magnetic field. This is due to an imbalance in the populations of left- and right-handed Weyl fermions [20,46].

This is the formula of the current fluctuation as a linear response of applied electric field:

$$Q^{zz}(i\Omega_n) = -\frac{e^2v_F^2}{4\pi^2l_B^2\hbar}\beta^{-1}\sum_{i\omega_n}\int_{-\infty}^{\infty}dk_z \times \mathrm{Tr}[\sigma^z G(i\omega_n + i\Omega_n, k_z)\sigma^z\Lambda(i\Omega_n)G(i\omega_n, k_z)]. \tag{22}$$

Here $G(i\Omega_n + i\omega_n, k_z) = \frac{1}{2}\{[g^+(i\Omega_n + i\omega_n, k_z) + g^-(i\Omega_n + i\omega_n, k_z)]\sigma^0 + [g^+(i\Omega_n + i\omega_n, k_z) - g^-(i\Omega_n + i\omega_n, k_z)]\sigma^z\}$, with $g^\pm(i\Omega_n + i\omega_n, k_z) = \frac{1}{i\Omega_n + i\omega_n + \mu \mp \hbar v_F k_z + \frac{i\mathrm{sgn}(i\Omega_n + i\omega_n)}{2\tau}}$. The symbol sgn is used for the sign function; $\mathrm{sgn}(x) = +1$ for $x > 0$, and $\mathrm{sgn}(x) = -1$ for $x < 0$. The current fluctuation formula is given in a finite-temperature Matsubara Green's function, with fermionic frequency $i\omega_n$ and bosonic frequency $i\Omega_n$. The symbol $l_B = \sqrt{\frac{\hbar}{eB}}$ is used for the magnetic length formed by Landau orbits.

The elastic scattering among Weyl fermions and impurities is considered. After scattering from impurity the chirality of the Weyl fermion is changed, for instance, from $\chi = +$ to $\chi = -$. The above formula for conductivity includes the ladder diagrams sum,

$$ev_F\sigma^z\Lambda(i\Omega_n) = ev_F\sigma^z + n_i\int_{-\infty}^{\infty}\frac{dk_z}{2\pi}|u(2k_z)|^2\{G(i\omega_n + i\Omega_n, k_z)[-ev_F\sigma^z\Lambda(i\Omega_n)]G(i\omega_n, k_z)\}. \tag{23}$$

We assume the impurities' influence is felt in the short range $|u(2k_z)| = |u|^2$, so the impurity potential $|u|^2$ is factored out of the integral:

$$\Lambda(i\Omega_n) = 1 - \frac{n_i|u|^2}{2\pi\hbar v_F}\Lambda(i\Omega_n)2\int_{-\infty}^{\infty}dx\left(\frac{1}{i\Omega_n + i\omega_n - x + \frac{i}{2\tau}\mathrm{sgn}(i\Omega_n + i\omega_n)}\frac{1}{i\omega_n - x + \frac{i}{2\tau}\mathrm{sgn}(i\omega_n)}\right). \tag{24}$$

The contour integral gives a nonzero value for this condition, $\mathrm{sgn}(i\Omega_n + i\omega_n) > 0$ and $\mathrm{sgn}(i\omega_n) < 0$. Here $\tau = \frac{2n_i|u|^2}{\hbar^2 v_F}$, and $x = \hbar v_F k_z$. After calculating the contour integral, we find

$$\Lambda(i\Omega_n) = \begin{cases} \frac{\Omega_n+\tau^{-1}}{\Omega_n+2\tau^{-1}} & \text{if } -i\Omega_n < i\omega_n < 0, \\ 1 & \text{otherwise.} \end{cases}$$

We use this in our formula for fluctuations in the current:

$$Q^{zz}(i\Omega_n) = -\frac{e^2 v_F}{4\pi^2 l_B^2 \hbar} 2\Lambda(i\Omega_n)\beta^{-1} \sum_{i\omega_n} \int_{-\infty}^{\infty} dx \left(\frac{1}{i\Omega_n + i\omega_n - x + \frac{i}{2\tau}\mathrm{sgn}(i\Omega_n + i\omega_n)} \frac{1}{i\omega_n - x + \frac{i}{2\tau}\mathrm{sgn}(i\omega_n)} \right), \tag{25}$$

$$Q^{zz}(i\Omega_n) = -\frac{e^2 v_F}{4\pi^2 L_B^2 \hbar} 2 \frac{\Omega_n + \tau^{-1}}{\Omega_n + 2\tau^{-1}} \beta^{-1} \sum_{-i\Omega_n < i\omega_n < 0} \frac{2i\pi}{i\Omega_n + i\tau^{-1}}. \tag{26}$$

Here $-\beta^{-1} \sum_{-i\Omega_n < i\omega_n < 0} 2i\pi = i\Omega_n$.

We analytically continue the above formula to get the conductivity: $\sigma_{zz}(i\Omega_n \to \Omega + i\delta) = \frac{Q^{zz}(\Omega+i\delta)}{\Omega}$,

$$\sigma_{zz}(i\Omega_n \to \Omega + i\delta) = \frac{e^2 v_F}{4\pi^2 l_B^2 \hbar} \frac{2}{2\tau^{-1} - i\Omega}. \tag{27}$$

This is the conductivity due to the chiral anomaly [14,20,30,51]:

$$\sigma_{zz}(\Omega = 0) = \frac{e^2 v_F}{4\pi^2 L_B^2 \hbar} \tau. \tag{28}$$

The other elements of the conductivity matrix are found in Ref. [32] (see also Refs. [14,52]). We only quote their results without deriving them, $\sigma_{xx} = \frac{A}{B}$, $\sigma_{xy} = \frac{nec}{B}$. Here A is a constant. This constant depends on the scattering time between Weyl or Dirac fermions and the charge impurities.

III. RESULTS AND DISCUSSION

A. Magnetoconductivity

In this section, we shall assume $\mu > \hbar\omega_c, k_B T$. The average deviation in the distribution function between opposite chiralities and the MC due to the chiral anomaly is shown in Fig. 2. This deviation in the distribution function arises due to the chiral anomaly and makes the magnetotransport properties different from the conventional semiclassical magnetotransport. This increases linearly with magnetic field and vanishes at $B = 0T$. The MC due to chiral anomaly increases quadratically with magnetic field.

In the plane perpendicular to the electric and magnetic fields the Lorentz force is balanced by the Coulomb force, and the Hall conductivity is observed. The inclusion of Berry curvature in the magnetotransport introduces a new comparison between the Lorentz and Berry curvature forces. Therefore, this study focuses on the plane of the electric and magnetic fields to see a comparison between the Berry curvature and Lorentz forces. The MC has a different functional dependence on these forces. It decreases for the Lorentz force but increases for the other. By varying the angle between these fields, we show the change in slope of the MC. This is shown in Fig. 3. The electric field angle is varied from the magnetic field axis at $\theta = 0$ to $\theta = \frac{\pi}{2}$. For a magnetic field applied perpendicular to the electric field, the MC decreases with increasing magnetic field: the familiar Boltzmann's equation result for the MC. By rotating the magnetic field to align with the electric field axis the MC slope starts increasing, and when both of the fields are parallel to each other, the MC slope is maximum. This effect is explained by the chiral anomaly, which enters into Boltzmann's equation from Berry curvature. It can be noticed that for some angles between the electric and magnetic fields the MC plot has a turning point. This turning point of the MC plot is an interesting point to

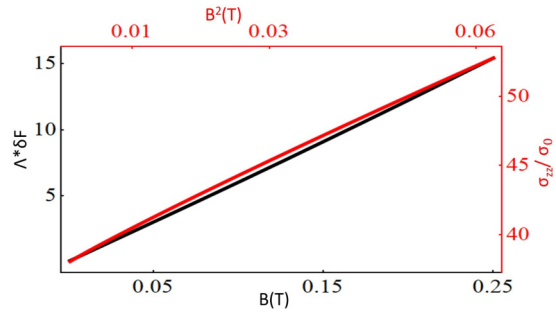

FIG. 2. The average deviation in the distribution function due to opposite chiralities and the MC due to the chiral anomaly. The different parameters are $\beta\mu = 5$, $\beta^2 e\hbar v_F^2 B = 90B/\mathrm{T}$, and $\Lambda = ev_F\tau_{tr}E_z/(2\pi^2\hbar^3 v_F^3\beta^2)$.

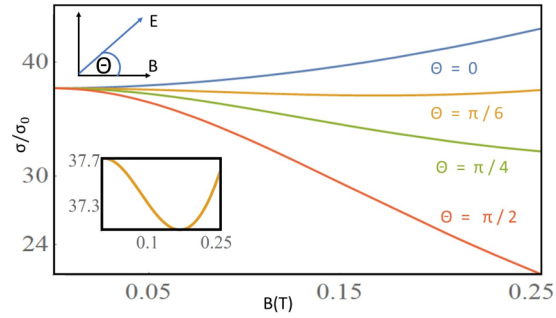

FIG. 3. The MC of the Weyl spectrum. The inset shows a magnified look at the MC vs the magnetic field characteristics. The different characteristics are plotted to show the comparative effect of the Lorentz force and the Berry force. The different parameters are $\beta\mu = 5$, $\beta e\tau_{tr} v_F^2 B = 20B/\mathrm{T}$, and $\beta^2 e\hbar v_F^2 B = 50B/\mathrm{T}$.

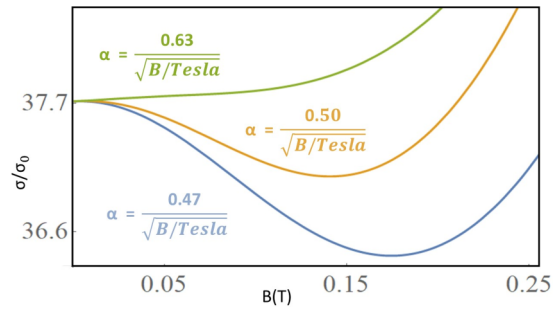

FIG. 4. The MC of Weyl spectrum. The different characteristics are plotted to show the relative strength of Lorentz force and the Berry force. The parameter: $\beta\mu = 5$.

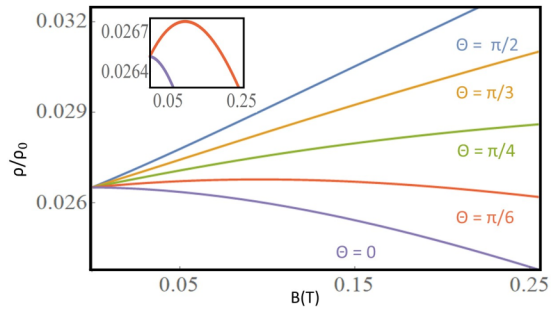

FIG. 6. The MR of the Weyl spectrum for the magnetic-field-dependent transport time. The different parameters are $\beta\mu = 5$, $\frac{\tau_{tr}}{\tau_s} = 0.9B/\mathrm{T}$, $\beta e\tau_{tr}v_F^2 B(1+0.9B/\mathrm{T})^{-1} = 20B(1+0.9B/\mathrm{T})^{-1}/\mathrm{T}$, and $\beta^2 e\hbar v_F^2 B = 45B/\mathrm{T}$.

see a comparison between the Lorentz force and the force arising due to Berry curvature. In Boltzmann's equation, the MC in the direction of the magnetic field has no magnetic field dependence, whereas in a plane perpendicular to the magnetic field the MC falls off with increasing magnetic field. This is the case for an electron gas with no chiral anomaly. But in a Weyl gas, the MC is dependent on magnetic field in every direction as a result of the chiral anomaly. A comparison of these two forces' strength is shown in Fig. 4 at fixed angle $\theta = \frac{\pi}{4}$. The ratio $\alpha = \sqrt{\frac{ev_F^2 B\hbar}{(ev_F^2 B\tau_{tr})^2}}$ shows the relative strength between these forces. The minima in the MC are tuned by this ratio. In this ratio α, $\hbar$ enters due to the Berry curvature, whereas τ_{tr} enters due to the Lorentz force. To detect this tuning experimentally, the transport time τ_{tr} can be changed by changing the mobility of the sample. The mobility of Weyl semimetals is a function of temperature and impurity concentration [27].

The MR in the semiclassical theory stays constant with changing magnetic field. However, it decreases due to the chiral anomaly with increasing magnetic field. This is shown in Fig. 5. The Berry curvature modifies the phase space [35]. Its effect is shown in the magnetoconductivity plot for $\theta = \frac{\pi}{2}$; here it should have a constant value (zero slope) if the Berry curvature is zero.

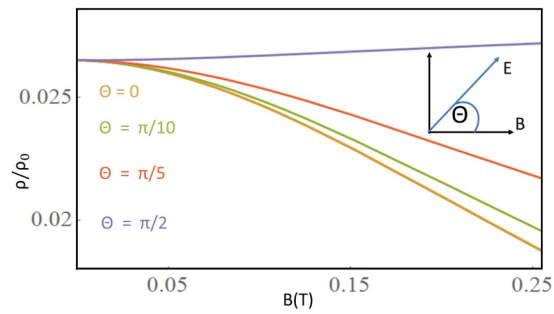

FIG. 5. The MR of the Weyl spectrum for the magnetic-field-independent transport time. The different characteristics show the MRs are dependent only on the Berry force, not on the Lorentz force. The different parameters are $\beta\mu = 5$, $\beta e\tau_{tr}v_F^2 B = 20B/\mathrm{T}$, and $\beta^2 e\hbar v_F^2 B = 90B/\mathrm{T}$.

B. Magnetic-field-dependent transport time

The experimental results of Weyl semimetals for the MR are not consistent with semiclassical theory for a magnetic-field-independent relaxation time [53]. Experimentally, the MR is often fit with Kohler's rule [54,55] and is shown to depend in detail on the shape of the Fermi surface. This explanation usually involves multiband models. In Dirac and Weyl semimetals the MR cannot be explained with the conventional multiband theory.

Here we find that the experimentally observed MR results for Weyl semimetals are well reproduced by assuming a linear magnetic field dependence in the charge transport rate. We do this by phenomenologically including the magnetic field dependence in the transport time. Here we motivate this assumption. A full calculation of the spin-dependent Boltzmann equation would be necessary to check this assumption. In support of this phenomenology of the magnetic-field-dependent relaxation time, we compare the spin precession time and momentum relaxation time of these materials. The momentum relaxation time depends on the mobility of the sample; high mobility results in a large relaxation time. Particularly in Weyl semimetals of mobility $\mu_B \sim 10^5 \frac{cm^2}{V-sec}$ the relaxation time is $\tau_{tr} \sim 10^{-13}$–10^{-14} s. The magnetic field of $B \sim 1T$ can precess a free electron within the time $\tau_s \sim 5 \times 10^{-12}$ s. In Weyl semimetals with a large Landé g factor $g \sim 10^2$ [56] the same magnetic field should precess an electron with the time $\tau_s \sim 10^{-14}$–10^{-13} s. This implies the momentum relaxation and the spin precession times are of the same order, $\tau_{tr} \sim \tau_s$. This is proposed in the semiclassical range since $\omega_c\tau_{tr} \sim 0.3 < 1$ for the magnetic field $B \sim 3$–5 T [57]. Another supporting argument in favor of the magnetic-field-dependent transport time in these materials within a semiclassical region is given in Ref. [31].

The above motivates us to include the magnetic field dependence in the relaxation time of the Weyl particle gas in a plane perpendicular to the magnetic field, $\frac{1}{\tau(B)} = \frac{1}{\tau_{tr}} + \frac{\Delta}{\hbar}$; otherwise, it stays constant, $\frac{1}{\tau(B)} = \frac{1}{\tau_{tr}}$.By including this magnetic-field-dependent relaxation time for MR, the resistivity element ρ_{xx} increases with the magnetic field, but the resistivity element ρ_{zz} decreases due to the chiral anomaly. Therefore, the slope of resistivity changes by rotating electric field from the magnetic field axis. This is shown in Fig. 6.

This maximum in the MR for angle $\theta = \frac{\pi}{6}$ between applied fields is due to the competition between the chiral anomaly and magnetic-field-dependent transport time. The MR plot qualitatively agrees with the experimental data of Ref. [27].

IV. CONCLUSION

In this study, we calculated the MC with both the Lorentz force and the Berry curvature force. For a finite angle between the electric and magnetic fields, the MC starts decreasing with increasing magnetic field due to the Lorentz force. It reaches the minimum point, and then it starts increasing due to the chiral anomaly. When these fields are orthogonal to each other, the MC plots show only a decrease with the magnetic field due to the Lorentz force. The MC increases rapidly with the magnetic field when both fields are in the same direction. This increase in the MC is an effect of the chiral anomaly (Fig. 3). This increase in the MC due to the chiral anomaly is quadratic (Fig. 2). The relative strength between the Lorentz and Berry curvature forces depends on the transport time. The chiral anomaly effect is more prominent in a clean sample (Fig. 4).

The plot of the MR does not show the effect of the Lorentz force within a single-band semiclassical theory. The diagonal elements of the MR show only an effect of the Berry force. Therefore, the transverse MR ρ_{xx} is almost constant (a slight change is caused by the modification of phase space with the magnetic field; Fig. 5). In this study, the transverse MR function's dependence on the magnetic field was made consistent with the experimental results by phenomenologically including the linear in magnetic field dependence in the transport time [27,36]. This is a plausible approximation for the relaxation mechanism of a distribution function. These results are valid for the high-mobility samples and with large Landé g factor. In these conditions, the momentum relaxation time and the spin precession time are of the same order within a semiclassical region [57]. We predict a linear increase in the transverse MR of high quality, and the large value of the Landé g factor sample is due to the spin precession. In future work we plan to solve the full spin Boltzmann equation to test this ansatz. We conclude by inviting experimentalists to detect the comparison between the Lorentz force and the Berry curvature force by avoiding Weyl semimetals that have a large Landé g factor. The MR element ρ_{xx} should be independent of magnetic field to detect the comparison between these forces within the semiclassical region.

APPENDIX: EQUATION OF MOTION DERIVATION

The formulas for the mean velocity and the Lorentz force of the Bloch wave packet are derived here. The equation of motion for the Bloch wave packet was derived by using the variational time-dependent principle [29,41,42]. Here we consider only the electromagnetic field coupling with the Bloch wave packet. The Bloch wave packet is formed by integrating the Bloch wave function over the Bloch wave vector $\hbar\vec{q}$:

$$|\psi\rangle = \int_{\vec{q}} |a(q,t)| \exp^{i[\vec{q}\cdot\hat{x} - \gamma(\vec{q},t)]} |u(\vec{q})\rangle, \tag{A1}$$

where $\gamma(\vec{q},t)$ is the phase of the Bloch wave packet and $|u(\vec{q})\rangle$ is the atomic part of the Bloch wave function. We are assuming a single-band Bloch wave function, so no index is needed to define different orbitals $|u_{n=1}(\vec{q})\rangle = |u(\vec{q})\rangle$. The Bloch wave packet is assumed to be normalized $\langle\psi|\psi\rangle = 1$. The spatial integral over the Bloch wave packet consists of two parts; the bigger part involves the whole crystal (our sample under investigation), and the smaller part involves only the unit cell, $\int_{\vec{x}} = \int_{\text{cell}} \times \int_{\text{crystal}}$. The formula for the Lagrangian of the Bloch wave packet is written by following the time-dependent variational principle:

$$L = \langle\psi|\left(i\hbar\frac{d}{dt} - H\right)|\psi\rangle. \tag{A2}$$

The first term gives

$$\begin{aligned}\langle\psi|i\hbar\frac{d}{dt}|\psi\rangle &= \int_{\vec{q}} |a(\vec{q},t)|^2 \frac{\partial\gamma(\vec{q},t)}{\partial t} \\ &= \frac{\partial\gamma(\vec{q}_c,t)}{\partial t}.\end{aligned} \tag{A3}$$

In the above equation we have used the fact that probability is not time dependent, $\frac{\partial}{\partial t}\int_{\vec{q}} |a(\vec{q},t)|^2 = 0$, and the Bloch wave packet is narrowly peaked in the unit cell. The time derivative of the Bloch wave packet phase $\frac{\partial}{\partial t}\gamma(\vec{q}_c,t)$ is related to its mean position $\vec{x}_c = \langle\psi|\hat{x}|\psi\rangle$ and the $\vec{q}$ dependence $\langle u(\vec{q})|i\frac{\partial}{\partial\vec{q}}u(\vec{q})\rangle$:

$$\begin{aligned}\langle\psi|\hat{x}|\psi\rangle = \int_{\vec{q},\vec{q}'} \delta(\vec{q}-\vec{q}')\Bigg\{&\frac{i}{2}\frac{\partial}{\partial\vec{q}}|a(\vec{q},t)|^2 + |a(\vec{q},t)|^2 \\ &\times\left[\frac{\partial}{\partial\vec{q}}\gamma(\vec{q},t) + \langle u(\vec{q})|i\frac{\partial}{\partial\vec{q}}u(\vec{q})\rangle\right]\Bigg\},\end{aligned} \tag{A4}$$

where the fact that probability is conserved also means $\int_{\vec{q}} \frac{\partial}{\partial\vec{q}}|a(\vec{q},t)|^2 = \delta|a(\vec{q},t)|^2 = 0$,

$$\langle\psi|\hat{x}|\psi\rangle = \int_{\vec{q}} |a(\vec{q},t)|^2\left[\frac{\partial}{\partial\vec{q}}\gamma(\vec{q},t) + \langle u(\vec{q})|i\frac{\partial}{\partial\vec{q}}u(\vec{q})\rangle\right], \tag{A5}$$

$$\vec{x}_c = \frac{\partial}{\partial\vec{q}_c}\gamma(\vec{q}_c,t) + \langle u(\vec{q}_c)|i\frac{\partial}{\partial\vec{q}_c}u(\vec{q}_c)\rangle. \tag{A6}$$

Adding a total time derivative function to a Lagrangian does not change the Euler's Lagrange equation:

$$\frac{d}{dt}\gamma(\vec{q}_c,t) = \dot{\vec{q}}_c\cdot\frac{\partial}{\partial\vec{q}_c}\gamma(\vec{q}_c,t) + \frac{\partial}{\partial t}\gamma(\vec{q}_c,t), \tag{A7}$$

$$\frac{\partial}{\partial t}\gamma(\vec{q}_c,t) = \frac{d}{dt}\gamma(\vec{q}_c,t) - \dot{\vec{q}}_c\cdot\vec{x}_c + \dot{\vec{q}}_c\cdot\langle u(\vec{q}_c)|i\frac{\partial}{\partial\vec{q}_c}u(\vec{q}_c)\rangle. \tag{A8}$$

This also implies $\frac{d}{dt}[\gamma(\vec{q}_c,t) - \vec{q}_c\cdot\vec{x}_c] = 0$. By using Eqs. (A3) and (A8),

$$\langle\psi|i\hbar\frac{d}{dt}|\psi\rangle = \vec{q}_c\cdot\dot{\vec{x}}_c + \dot{\vec{q}}_c\cdot\langle u(\vec{q}_c)|i\frac{\partial}{\partial\vec{q}_c}u(\vec{q}_c)\rangle. \tag{A9}$$

Now we shall include the coupling of the electromagnetic fields $[\phi(\vec{x},t), A(\vec{x},t)]$ with the Bloch wave packet. This will modify the Bloch wave vector $\vec{q}$ into the gauge-invariant Bloch wave vector $\vec{k} = \vec{q} + e\vec{A}(\vec{x},t)$.

This is the expectation value of the Hamiltonian,

$$\langle\psi|H|\psi\rangle = \epsilon_{\vec{M}} - e\phi(\vec{x}_c, t). \tag{A10}$$

Here $\epsilon_{\vec{M}} = \epsilon_{\vec{k}_c} - \vec{M}\cdot\vec{B}$, and $\vec{M}$ is the orbital magnetization. The orbital magnetization gives the perturbation correction in the energy. In our calculation of magnetotransport the orbital magnetization effect is ignored.

By using Eqs. (A9) and (A10) in Eq. (A2), we derive the Lagrangian of Bloch wave packet:

$$\begin{aligned} L(\vec{x}_c, \dot{\vec{x}}_c, \vec{k}_c, \dot{\vec{k}}_c, t) = &-\epsilon_{\vec{M}} + e\phi(\vec{x}_c, t) \\ &+ \dot{\vec{x}}_c \cdot [\vec{k}_c - e\vec{A}(\vec{x}_c, t)] \\ &+ \dot{\vec{k}}_c \cdot \langle u(\vec{k}_c)| i\frac{\partial}{\partial \vec{k}_c} u(\vec{k}_c)\rangle. \end{aligned} \tag{A11}$$

The Lorentz force acting on the Bloch wave packet is derived by using Euler's Lagrange equation of the canonical conjugate pair $[\vec{x}_c, \dot{\vec{x}}_c]$:

$$\frac{d}{dt}\frac{\partial L}{\partial \dot{\vec{x}}_c} = \frac{\partial L}{\partial \vec{x}_c}, \tag{A12}$$

$$\frac{\partial L}{\partial x_c^j} = e\frac{\partial \phi(\vec{x}_c, t)}{\partial x_c^j} - e\dot{x}_c^i \frac{\partial A^i(\vec{x}_c, t)}{\partial x_c^j}, \tag{A13}$$

$$\frac{d}{dt}\frac{\partial L}{\partial \dot{x}_c^j} = \delta^{ij}\left(\hbar\dot{k}_c^i - e\frac{\partial A^i(\vec{x}_c, t)}{\partial t} - e\dot{x}_c^k \frac{A^i(\vec{x}_c, t)}{\partial x_c^k}\right), \tag{A14}$$

$$\hbar\dot{\vec{k}} = -e(\vec{E} + \dot{\vec{x}}_c \wedge \vec{B}). \tag{A15}$$

Also, the formula for the mean velocity of the Bloch wave packet is derived by using Euler's Lagrange equation for the canonical conjugate pair $[\hbar\vec{k}_c, \hbar\dot{\vec{k}}_c]$:

$$\frac{1}{\hbar}\frac{d}{dt}\frac{\partial L}{\partial \dot{\vec{k}}_c} = \frac{1}{\hbar}\frac{\partial L}{\partial \vec{k}_c}, \tag{A16}$$

$$\frac{1}{\hbar}\frac{\partial L}{\partial k_c^i} = -\frac{1}{\hbar}\frac{\partial \epsilon_{\vec{M}}}{\partial k^i} + \dot{x}^j \delta^{ij}, \tag{A17}$$

$$\frac{1}{\hbar}\frac{d}{dt}\frac{\partial L}{\partial \dot{k}_c^i} = i\frac{d}{dt}\langle u(\vec{k}_c)\left|\frac{\partial u(\vec{k}_c)}{\partial k_c^j}\right\rangle \delta^{ij}, \tag{A18}$$

$$\begin{aligned} i\frac{d}{dt}\langle u(\vec{k}_c)\left|\frac{\partial u(\vec{k}_c)}{\partial k_c^j}\right\rangle = i\dot{k}_c^i\Bigg(&\left\langle \frac{\partial u(\vec{k}_c)}{\partial k_c^i}\middle|\frac{\partial u(\vec{k}_c)}{\partial k_c^j}\right\rangle \\ &- \left\langle \frac{\partial u(\vec{k}_c)}{\partial k_c^j}\middle|\frac{\partial u(\vec{k}_c)}{\partial k_c^i}\right\rangle\Bigg). \end{aligned} \tag{A19}$$

Let's define Berry curvature:

$$\Omega_n^k = i\left(\left\langle \frac{\partial u(\vec{k}_c)}{\partial k_c^i}\middle|\frac{\partial u(\vec{k}_c)}{\partial k_c^j}\right\rangle - \left\langle \frac{\partial u(\vec{k}_c)}{\partial k_c^j}\middle|\frac{\partial u(\vec{k}_c)}{\partial k_c^i}\right\rangle\right). \tag{A20}$$

Therefore, anomalous velocity enters into the equation of motion of the mean position of the Bloch wave packet $\vec{x}_c$:

$$\dot{\vec{x}}_c = \vec{v} - \dot{\vec{k}}_c \wedge \vec{\Omega}. \tag{A21}$$

Here $\vec{v} = \frac{1}{\hbar}\vec{\nabla}_k \epsilon_{\vec{M}}$. The anomalous velocity $\dot{\vec{k}}_c \wedge \vec{\Omega}$ is the Lorentz force in momentum space:

$$\hbar\dot{\vec{k}}_c = -e(\vec{E} + \dot{\vec{x}}_c \wedge \vec{B}), \tag{A22}$$

$$\dot{\vec{x}}_c = \vec{v} - \dot{\vec{k}}_c \wedge \vec{\Omega}. \tag{A23}$$

One can uncouple these equations by using vector cross-product properties $(\vec{A}\wedge\vec{B})\wedge\vec{C} = (\vec{A}\cdot\vec{C})\vec{B} - (\vec{B}\cdot\vec{C})\vec{A}$:

$$\dot{\vec{x}}_c = \frac{1}{1 + \frac{e\vec{B}\cdot\vec{\Omega}}{\hbar}}[\vec{v} - \frac{e}{\hbar}\vec{E}\wedge\vec{\Omega} + \frac{e}{\hbar}(\vec{\Omega}\cdot\vec{v})\vec{B}], \tag{A24}$$

$$\hbar\dot{\vec{k}}_c = \frac{1}{1 + \frac{e\vec{B}\cdot\vec{\Omega}}{\hbar}}[e\vec{E} + e\vec{v}\wedge\vec{B} + \frac{e^2}{\hbar}(\vec{E}\cdot\vec{B})\vec{\Omega}]. \tag{A25}$$

These are the formulas of the mean velocity $\dot{\vec{x}}_c$ and the Lorentz force $\hbar\dot{\vec{k}}_c$ of the Bloch wave packet.

[1] H. Weyl, Z. Phys. **56**, 330 (1929).
[2] T. Kajita, Rev. Mod. Phys. **88**, 030501 (2016).
[3] A. B. McDonald, Rev. Mod. Phys. **88**, 030502 (2016).
[4] A. H. Castro Neto, F. Guinea, N. M. R. Peres, K. S. Novoselov, and A. K. Geim, Rev. Mod. Phys. **81**, 109 (2009).
[5] S. M. Young, S. Zaheer, J. C. Y. Teo, C. L. Kane, E. J. Mele, and A. M. Rappe, Phys. Rev. Lett. **108**, 140405 (2012).
[6] B. A. Bernevig and T. L. Hughes, *Topological Insulators and Topological Superconductors* (Princeton University Press, Princeton, NJ, 2013).
[7] M. Z. Hasan, S.-Y. Xu, I. Belopolski, and S.-M. Huang, Annu. Rev. Condens. Matter Phys. **8**, 289 (2017).
[8] X. Wan, A. M. Turner, A. Vishwanath, and S. Y. Savrasov, Phys. Rev. B **83**, 205101 (2011).
[9] C.-L. Zhang, S.-Y. Xu, I. Belopolski, Z. Yuan, Z. Lin, B. Tong, G. Bian, N. Alidoust, C.-C. Lee, S.-M. Huang, T.-R. Chang, G. Chang, C.-H. Hsu, H.-T. Jeng, M. Neupane, D. S. Sanchez, H. Zheng, J. Wang, H. Lin, C. Zhang, H.-Z. Lu, S.-Q. Shen, T. Neupert, M. Z. Hasan, and S. Jia, Nat. Commun. **7**, 10735 (2016).
[10] S.-Y. Xu, N. Alidoust, I. Belopolski, C. Zhang, G. Bian, T.-R. Chang, H. Zheng, V. Strokov, D. S. Sanchez, G. Chang, Z. Yuan, D. Mou, Y. Wu, L. Huang, C.-C. Lee, S.-M. Huang, B. Wang, A. Bansil, H.-T. Jeng, T. Neupert, A. Kaminski, H. Lin, S. Jia, and M. Z. Hasan, Nat. Phys. **11**, 748 (2015).
[11] S.-Y. Xu, I. Belopolski, N. Alidoust, M. Neupane, C. Zhang, R. Sankar, S.-M. Huang, C.-C. Lee, G. Chang, B. Wang, G. Bian, H. Zheng, D. S. Sanchez, F. Chou, H. Lin, S. Jia, and M. Z. Hasan, Science **349**, 613 (2015).
[12] K. Kuroda, T. Tomita, M.-T. Suzuki, C. Bareille, A. A. Nugroho, P. Goswami, M. Ochi, M. Ikhlas, M. Nakayama, S. Akebi, R. Noguchi, R. Ishii, N. Inami, K. Ono, H. Kumigashira, A. Varykhalov, T. Muro, T. Koretsune, R. Arita, S. Shin, Takeshi Kondo, and S. Nakatsuji, Nat. Mater. **16**, 1090 (2017).
[13] X. Dai, Z. Z. Du, and H. Z. Lu, Phys. Rev. Lett. **119**, 166601 (2017).

[14] J. Klier, I. V. Gornyi, and A. D. Mirlin, Phys. Rev. B **96**, 214209 (2017).

[15] A. A. Soluyanov, Physics **10**, 74 (2017).

[16] S. Tchoumakov, M. Civelli, and M. O. Goerbig, Phys. Rev. Lett. **117**, 086402 (2016).

[17] S.-Y. Xu, N. Alidoust, G. Chang, H. Lu, B. Singh, I. Belopolski, D. S. Sanchez, X. Zhang, G. Bian, H. Zheng, M.-A. Husanu, Y. Bian, S.-M. Huang, C.-H. Hsu, T.-R. Chang, H.-T. Jeng, A. Bansil, T. Neupert, Vl. N. Strocov, H. Lin, S. Jia, and M. Z. Hasan, Sci. Adv. **3**, e1603266 (2017).

[18] M. Z. Hasan and C. L. Kane, Rev. Mod. Phys. **82**, 3045 (2010).

[19] G. Volovik, *The Universe in a Helium Droplet* (Clarendon, Oxford, 2003).

[20] H. Nielssen and N. Ninomiya, Phys. Lett. B **130**, 389 (1983).

[21] N. Armitage, E. Mele, and A. Vishwanath, Rev. Mod. Phys. **90**, 015001 (2018).

[22] G. Basar, D. E. Kharzeev, and H. U. Yee, Phys. Rev. B **89**, 035142 (2014).

[23] M. A. Stephanov and Y. Yin, Phys. Rev. Lett. **109**, 162001 (2012).

[24] D. T. Son and N. Yamamoto, Phys. Rev. Lett. **109**, 181602 (2012).

[25] K. Landsteiner, E. Megias, and F. Pena-Benitez, Phys. Rev. Lett. **107**, 021601 (2011).

[26] J. F. Steiner, A. V. Andreev, and D. A. Pesin, Phys. Rev. Lett. **119**, 036601 (2017).

[27] H. Li, H. He, H.-Z. Lu, H. Zhang, H. Liu, R. Ma, Z. Fan, S.-Q. Shen, and J. Wang, Nat. Commun. **7**, 10301 (2016).

[28] A. A. Zyuzin and A. A. Burkov, Phys. Rev. B **86**, 115133 (2012).

[29] K.-S. Kim, H.-J. Kim, and M. Sasaki, Phys. Rev. B **89**, 195137 (2014).

[30] G. Sundaram and Q. Niu, Phys. Rev. B **59**, 14915 (1999).

[31] J. C. W. Song, G. Refael, and P. A. Lee, Phys. Rev. B **92**, 180204 (2015).

[32] A. A. Abrikosov, Phys. Rev. B **58**, 2788 (1998).

[33] V. A. Zyuzin, Phys. Rev. B **95**, 245128 (2017).

[34] G. Sharma, P. Goswami, and S. Tewari, Phys. Rev. B **93**, 035116 (2016).

[35] D. Xiao, J. Shi, and Q. Niu, Phys. Rev. Lett. **95**, 137204 (2005).

[36] M. Hirschberger, S. Kushwaha, Z. Wang, Q. Gibson, S. Liang, C. A. Belvin, B. A. Bernevig, R. J. Cava, and N. P. Ong, Nat. Mater. **15**, 1161 (2016).

[37] H.-J. Kim, K.-S. Kim, J.-F. Wang, M. Sasaki, N. Satoh, A. Ohnishi, M. Kitaura, M. Yang, and L. Li, Phys. Rev. Lett. **111**, 246603 (2013).

[38] X. Huang, L. Zhao, Y. Long, P. Wang, D. Chen, Z. Yang, H. Liang, M. Xue, H. Weng, Z. Fang, X. Dai, and G. Chen, Phys. Rev. X **5**, 031023 (2015).

[39] J. Xiong, S. K. Kushwaha, T. Liang, J. W. Krizan, M. Hirschberger, W. Wang, R. J. Cava, and N. P. Ong, Science **350**, 413 (2015).

[40] Q. Li, Dmitri E. Kharzeev, C. Zhang, Y. Huang, I. Pletikosic, A. V. Fedorov, R. D. Zhong, J. A. Schneeloch, G. D. Gu, and T. Valla, Nat. Phys. **12**, 550 (2016).

[41] D. Xiao, M. C. Chang, and Q. Niu, Rev. Mod. Phys. **82**, 1959 (2010).

[42] M. P. Marder, *Condensed Matter Physics* (Wiley, Hoboken, NJ, 2010).

[43] H. R. Chang, J. Zhou, S. X. Wang, W. Y. Shan, and D. Xiao, Phys. Rev. B **92**, 241103 (2015).

[44] M. M. Vazifeh and M. Franz, Phys. Rev. Lett. **111**, 027201 (2013).

[45] H. Weng, C. Fang, Z. Fang, B. A. Bernevig, and X. Dai, Phys. Rev. X **5**, 011029 (2015).

[46] D. T. Son and B. Z. Spivak, Phys. Rev. B **88**, 104412 (2013).

[47] J. Xiong, S. Kushwaha, J. Krizan, T. Liang, R. J. Cava, and N. P. Ong, Europhys. Lett. **97**, 67004 (2012).

[48] P. E. C. Ashby and J. P. Carbotte, Phys. Rev. B **89**, 245121 (2014).

[49] C. J. Tabert and J. P. Carbotte, Phys. Rev. B **93**, 085442 (2016).

[50] L. M. Schoop, M. N. Ali, C. Straßer, A. Topp, A. Varykhalov, D. Marchenko, V. Duppel, S. S. P. Parkin, B. V. Lotsch, and C. R. Ast, Nat. Commun. **7**, 11696 (2016).

[51] V. Aji, Phys. Rev. B **85**, 241101 (2012).

[52] X. Xiao, K. T. Law, and P. A. Lee, Phys. Rev. B **96**, 165101 (2017).

[53] C.-Z. Li, L.-X. Wang, H. Liu, J. Wang, Z.-M. Liao, and D.-P. Yu, Nat. Commun. **6**, 10137 (2015).

[54] J. L. Olsen, *Electron Transport in Metals* (Interscience Publishers, New York, 1962).

[55] M. Kohler, Ann. Phys. (Berlin, Ger.) **424**, 211 (1938).

[56] S. Jeon, B. B. Zhou, A. Gyenis, B. E. Feldman, I. Kimchi, A. C. Potter, Q. D. Gibson, R. J. Cava, A. Vishwanath, and A. Yazdani, Nat. Mater. **13**, 851 (2014).

[57] S. Nandy, G. Sharma, A. Taraphder, and S. Tewari, Phys. Rev. Lett. **119**, 176804 (2017).